LAWRENCE
LIVERMORE
NATIONAL
LABORATORY

UCRL-JRNL-213370

Sea Water Radiocarbon Evolution in the Gulf of Alaska: 2002 Observations

T. P. Guilderson, E. B. Roark, P. D. Quay, S. R. Flood-Page, C. Moy

July 1, 2005

Radiocarbon

Sea Water Radiocarbon Evolution in the Gulf of Alaska: 2002 Observations

T.P. Guilderson[1,2], E.B. Roark[3], P.D. Quay[4] , S.R. Flood-Page[5], C. Moy[6]

[1] Center for Accelerator Mass Spectrometry, LLNL, Livermore CA 94551, USA.
[2] Department of Ocean Sciences, University of California – Santa Cruz, Santa Cruz CA 94056, USA.
[3] Department of Geography, University of California – Berkeley, Berkeley CA 94720, USA.
[4] School of Oceanography, University of Washington, Seattle WA 98195, USA.
[5] Department of Biological Sciences, University of California – Santa Cruz, Santa Cruz CA 94056, USA.
[6] Department of Geological and Environmental Sciences, Stanford University, Stanford CA 94305, USA.

Radiocarbon
Intended submission date: 4/28/2005

ABSTRACT

Oceanic uptake and transport of bomb radiocarbon as $^{14}CO_2$ created by atmospheric nuclear weapons testing in the 1950s and 1960s has been a useful diagnostic to determine the carbon transfer between the ocean and atmosphere. In addition, the distribution of radiocarbon in the ocean can be used as a tracer of oceanic circulation. Results obtained from samples collected in the Gulf of Alaska in the summer of 2002 provide a direct comparison with results in the 1970s during GEOSECS and in the early 1990s during WOCE. The open gyre values are 20-40‰ more negative than those documented in 1991 and 1993 (WOCE) although the general trends as a function of latitude are reproduced. Surface values are still significantly higher than pre-bomb levels (~-105‰ or lower). In the central gyre, we observe $\Delta^{14}C$-values that are lower in comparison to GEOSECS (stn 218) and WOCE P16/P17 to a density of ~26.8σt. This observation is consistent with the overall decrease in surface $\Delta^{14}C$ values, and reflects the erosion of the bomb-^{14}C transient. We propose that erosion of the bomb-^{14}C transient is accomplished by entrainment of low^{14}C water via vertical exchange within the Gulf of Alaska and replenishment of surface and sub-thermocline waters with waters derived from the far northwest Pacific.

INTRODUCTION

Due to the long radioactive half-life the oceanic distribution of natural radiocarbon (^{14}C expressed as $\Delta^{14}C$; (Stuiver and Polach, 1977)) reflects centennial to

millennial scale circulation. Atmospheric nuclear testing in the 1950s and early 1960s resulted in an excess of ^{14}C which augmented the natural ^{14}C gradient between surface and subsurface waters. This contrast makes the distribution of radiocarbon in the surface ocean particularly sensitive to vertical mixing and lateral exchange. Oceanic uptake and transport of bomb radiocarbon as $^{14}CO_2$ has been a useful diagnostic to determine the carbon transfer between the ocean and atmosphere and as a transient tracer of ocean circulation. The present-day distribution of bomb radiocarbon in the ocean reflects the integration of variable circulation and air-sea exchange over the last ~45 years.

We present $\Delta^{14}C$ data of the total dissolved inorganic carbon (ΣCO_2) determined on surface water and two hydro-casts collected in June/July of 2002 in the Gulf of Alaska. These results are compared with similar $\Delta^{14}C$ data obtained during WOCE sections P16n (1991), P17n (1993), opportunistic cruises in the 1980s, and GEOSECS station 218 in 1973 .

North Pacific Circulation

In general the shallow sub-subsurface circulation of the sub-polar North Pacific tends to follow the wind-driven circulation creating a large subpolar cyclonic gyre north of 40 degrees (Figure 1) (*cf.* Sverdrup *et al.*, 1942; Reid and Arthur, 1975). The southern edge of the sub-arctic gyre is delineated by the eastward flowing North Pacific Current, which is sourced in the far west from the Kuroshio Current. The Gulf of Alaska contains the third, and eastern-most of the sub-arctic cyclonic gyres imbedded in the over all cyclonic gyre of the subarctic. The Alaskan gyre is bounded to the east by the Alaskan Current, which east of Kodiak Island converges with the strong westward flowing Alaskan Stream. The western boundary is nominally at 180° where the Aleutian Islands dip furthest south and force the Alaskan Stream south, essentially closing the small gyre. In the Gulf of Alaska, and the whole of the subpolar North Pacific, low surface water salinity maintain a large density contrast which in general suppresses deep convection. Climatological winter mixed layer depths are on the order of 100-200 meters (Monterey and Levitus, 1997). West to east across the subpolar North Pacific, isopycnals trend

downward (Figure 1). Coastal downwelling and deepening of isopycnals to the south of the Alaskan Gyre dominate the north south trend (Figure 1). Bowing up of the isopycnals in the center of the gyre along the meridional profile is consistent with wind driven Ekman divergence and the large-scale North Pacific wind-field.

There are relatively few easily characterizable sub-surface water masses in the North Pacific. A major sub-thermocline water type is North Pacific Intermediate Water (NPIW) which is characterized by low salinities (~33.9 psu) and high oxygen content (e.g., Talley, 1991; Talley et al., 1991; Tsunogai et al., 1995). Utilizing salinity and oxygen to define it places the core of this water mass at a potential density (σ_t) of 26.8 kg/m^3. NPIW is one of the major interior water masses of the North Pacific and its fundamental characteristics can be traced to ~20°N and along Baja to near the equator. Waters of this density (in a climatological sense) do not outcrop in the open subpolar North Pacific and it has been determined that the source of much of this water is from the Sea of Okhotsk (Talley 1991; Talley et al., 1991). The northern extent of NPIW is delimited by the subarctic front except in the east where a tongue of low salinity water at the appropriate density is found around the eastern side of the Gulf of Alaksa (Talley 1993).

Transient tracers such as chlorofluorocarbon and "bomb" derived tritium and radiocarbon data indicate that NPIW waters are in general a few decades old (e.g., Watanabe et al., 1994; Warner et al., 1996; Tsunogai et al., 1995; Van Scoy et al., 1991a) and that the circulation follows that of the surface waters, albeit offset slightly to the east and south. The tracer data indicates that direct air-sea exchange in the open North Pacific is limited, with most of NPIW being formed in the Sea of Okhotsk. However, in their analysis of transient tracer data Van Scoy et al. (1991b) inferred that there does appear to be wintertime ventilation in the Gulf of Alaska with sufficient vigor as to mix into NPIW. Subsequent analysis of WOCE P17 chlorofluorocarbon and hydrographic data collected in 1993 (Aydin et al., 1998) imply modification of NPIW and subsurface waters within the Gulf of Alaska and the Alaskan gyre in particular.

METHODS

Water samples were collected in June and July of 2002 during the Gulf of Alaska Seamount Expedition (GoASEx-2002) on the RV/Atlantis (ATL 7/15 and ATL 7/16: Figure 2). Underway samples were taken from the vessel's continuous flow clean seawater line after purging the line for at least 5 minutes before collection. Two sets of hydrocast samples were collected using a niskin-CTD array at Patton (ATL 7-15 ctd1: 53.93°N, 148.43°W) and Warwick (ATL7-16 ctd2: 47.95°N, 132.92°W) Seamounts. Half-litre glass bottles were filled from the bottom and allowed to flush for twice their volume prior to poisoning with mercuric chloride and storage. Following standard protocols, total dissolved inorganic carbon was quantitatively stripped via acidification and purging with nitrogen at the School of Oceanography, University of Washington (UW). Aliquots of cryogenically purified CO_2 were analyzed for $\delta^{13}C$ at UW and the remaining CO_2 transferred to the Center for AMS in glass ampules.

CO_2 was reduced to elemental graphite in the presence of iron catalyst and a stoichiometric excess of hydrogen similar to the method described by Vogel et al., (1987). Graphite targets were measured at CAMS. Raw data ($^{14}C/^{13}C$ ratios) are normalized to the average of six bracketing aliquots of the primary standard (OX-1) for each pass through a sample group. Counting errors (primary standard and unknown) are propagated through the analysis and are assumed to be Gaussian (cf. Bevington and Robinson, 1992). The average of the n-measurement-cycles of each unknown is then determined and for the final error, the larger of the counting error or the external error of the n-cycles is chosen. CAMS ^{14}C data are based on $^{14}C/^{13}C$ atom ratios not decay counting to obtain specific ^{14}C activities. The algorithms used (Southon unpublished) are similar to those developed at Arizona (Donahue, Linick, and Jull, 1990). Radiocarbon results are reported as *absolute* fraction modern and equivalent age-corrected $\Delta^{14}C$ (‰) as defined by Stuiver and Polach (1977) and include a background subtraction and the $\delta^{13}C$ correction obtained from the stable isotope results. The majority of samples were analyzed in conventional mode to a fractional precision level of ~±3.0‰ (1σ).

We took advantage of a subset of the ampoules as a means to test the limits of AMS-^{14}C analytical precision. For these samples we made two individual (~60μmole-C) graphite targets from the single CO_2 ampoule. The graphite targets were then analyzed in what is now being termed "ultra-precision" mode. Each wheel load is composed of a suite of about ten aliquots of the primary (OX1) standard, a single set of secondary standards (OX2, ANU, TIRI B wood), the unknown samples and blanks; and is broken into several groups. In general, a group is composed of 10-14 unknowns with intervening and bracketing primary standards. Samples are analyzed in such a fashion that a single group is completely analyzed prior to proceeding onto the next. A group is analyzed repeatedly such that a suite of bracketing primary standards and the secondary standards are analyzed in conjunction with the unknown samples. For "ultra-precision" samples, 10 unknowns compose a group. Additional secondary standards were analyzed amongst, and as unknowns. During each cycle an individual target was analyzed for 50,000 ^{14}C events. Initially we had intended on cycling all of the ultra-precision targets at least 20 times (*ie*., 1x10^6 ^{14}C events) but beam-time considerations precluded this. The last set of "ultra-precision" samples were only analyzed for ~7.5x10^5 ^{14}C events.

RESULTS

The southern boundary of the sub-polar gyre is approximately demarked by the zero-line of the curl of the wind-stress. To estimate the southern end of the gyre we calculated the zero line of the curl of the wind stress using a simple bulk formula approximation of the u/v stress and the average May-June 2002 surface u and v wind velocities provided by the NCEP reanalysis (cdc.noaa.gov). In this case we calculated pseudo-stress; for u-vector this is given by $\tau_u = \rho_a * C_d * abs(U) * U$ where ρ_a is the density of air, C_d is a unit-less drag coefficient ~1.4x10^{-3}, and U is the u-component of the wind velocity. The southern-most stations, are likely to have been either outside the gyre or at the gyre boundary in the North Pacific Current (Figure 2). This would be comparable with Western Subpolar Water and the transition zone described in Aydin et al., (1998).

Fundamental oceanographic and carbon isotope data are tabulated in tables 1,2, and 3. Table 1 contains the under-way surface data, and table 2 and 3 contain the results from the two hydrocasts. For the most part, sea surface temperature (SST) and salinity (SSS) are strongly correlated (Figure 3). Temperatures decrease from ~13°C to ~9°C from 47.5°N to 54°N before rising to ~12°C as one crosses into the Alaskan Stream heading in towards Kodiak. Salinity steadily increases over the same latitudinal range from a low of ~32.1 at 47.5°N to a high of ~33, again at 54°N. Salinity dramatically decreases as one exits the Alaskan gyre and heads north towards Kodiak.

Surface water $\Delta^{14}C$ values as a function of latitude have a pronounced "v-shape" (Figure 4). The highest values that we observed (~ +20‰) were at the southward edge of the Alaskan Gyre (47.5°N) and the lowest values (~ -20‰) at 55°N. Further north as one crosses the Alaskan Stream, values increase to ~+10‰. The open gyre values are 20-40‰ more negative than those documented in 1991 and 1993 (WOCE; data of Key *et al.*, 1996) although the general trends are reproduced.

Vertical profiles of temperature, salinity, oxygen, and $\Delta^{14}C$ at Patton and Warwick Seamounts (Figure 5) exhibit common features; strong halocline, sub-surface temperature maximum, thick oxygen minimum zone, and a sub-surface oxygen maximum above the main halocline. At Patton temperatures decrease from ~9°C at the surface to ~3.4°C at ~80meters. The main thermocline is at ~27meters. There is a sub-surface temperature maximum of ~4°C at ~140m near the base of the halocline. Below the sub-surface maximum, temperature decreases to ~1.6°C at 2200 meters. Salinity increases from ~33.00 at the surface through a mini-halocline at ~25m, where values become nearly constant at 33.14 between ~50 and ~80 meters. The main halocline is at 110m (33.50) and rolls over at ~140meters (33.84), after which salinity gently increases with depth to 34.62 at 2200 meters. Surface water oxygen concentration at Patton is ~276μmole/kg. Oxygen concentration increases with depth through the main thermocline to a subsurface maximum of ~314μm/kg at 30 meters. Oxygen remains high until ~80meters and then decrease in a two-step fashion across the main halocline. Oxygen values at Patton are

low (8.2-10.2μm/kg) between ~200m and ~800m and then increase with depth to 78μm/kg by 2200meters.

Temperature at Warwick decreases from 12.9°C at the surface through the main thermocline (~40 meters) to ~7.2°C at 50 meters. Temperature slowly decreases to ~5.8°C at 110m where a ~20 meter thermostad is observed. Temperature increases below the thermstad (~130m) to a sub-surface maximum of ~6.4°C at ~185 meters. Except for a slight pause at ~850meters, temperature decreases steadily to ~1.8°C at 2200meters. Salinity slowly increases from 32.38 at the surface to 32.65 at the top of the halocline (120 meters). The main halocline is at 140 meters and rolls over by 185 meters (33.79). Salinity gradually increases to 33.91 at 340 meters and then increases in a more regular fashion to 34.60 at 2200 meters. Oxygen concentrations increase from 264μmolar at the surface to a sub-surface maximum of 302μmole/kg at 42 meters and high oxygen concentrations to the halocline. Below the halocline oxygen concentration rapidly decreases to a 300 meter thick oxygen minimum (2.8-5.5 μm/kg) zone between ~800 and ~1100 meters. Oxygen concentration increases to ~64μm/kg by 2200 meters.

In both profiles there is a well-mixed (with respect to $\Delta^{14}C$) surface layer. At Patton this layer is to at least 50m but less than 100m and would be consistent with the depth of the main thermocline, but not through the main halocline. At Warwick the constant $\Delta^{14}C$ layer penetrates into the main halocline and extends to ~150m. Below the surface mixed layer, values decrease as a function of depth. The minimum observed $\Delta^{14}C$ value at Patton Seamount is -239‰ and -237‰ at Warwick Seamount. The minima are not observed in the oxygen minimum zone but the water mass below it. Corresponding $\Delta^{14}C$ in the Patton Seamount bottle samples with the lowest oxygen content are ~ -190‰, and the one sample at Warwick is -183‰.

The "ultra-precision" replicates were determined over the span of three different sample wheels and two different AMS runs and include both "within" wheel and between wheel replicates – *i.e.*, a realistic albeit limited test of external variability. As discussed in the methods section, due to beam-time limitations some of the samples were only

analyzed for ≥7.5x10^5 ^{14}C events, not the full ≥1x10^6. The average fractional error of the thirty-three pairs of targets is 0.94‰ (Figure 6). The majority of the pairs replicate within 1-σ, two pairs at 2-σ, and the third will keep us honest.

DISCUSSION

Evolution of ^{14}C and Ocean Circulation

Surface Δ^{14}C has a somewhat simpler albeit noisier linear relationship to temperature than salinity. Higher Δ^{14}C is observed at warmer temperatures with low Δ^{14}C corresponding with cooler and saltier waters. This results in a near linear relation between Δ^{14}C and potential density (Figure 4). In density space, Δ^{14}C of the Alaskan Stream (stations north of 55°) are indistinguishable from stations in the middle of the gyre (50° - 53°N). These Δ^{14}C values are intermediate between the low values observed towards 55°N and the high Δ^{14}C at the warm fresh end to the south. This gives the distinct impression of a simple two end-member mixing model between a low-^{14}C end-member at ~25.5 kg-cc^{-3} and a high-^{14}C end member <24.5 kg-cc^{-3}. If the Alaskan Current sources from water at the southern gyre boundary our limited data indicates that there is addition of low ^{14}C water through vertical entrainment or from freshwater coastal run-off. This water then requires density modification to fit the simple two end-member mixing model. In the case of vertical entrainment this could be accomplished through radiative heating and freshening to decrease the salinity of sub-surface saltier waters. In the case of coastal (freshwater) run-off, evaporation would be required to increase the salt content. Freshwater run-off is likely to have a Δ^{14}C signature similar to the atmosphere, which is higher than surface Gulf of Alaska surface waters. Thus freshwater run-off would be a relative source of more positive Δ^{14}C. If the Alaskan Current is primarily sourced from southern gyre waters the data imply that there is little modification of the ^{14}C content in the Alaskan Current/Stream, at least during late spring and into early summer. Additionally, this would not require adding/removing salt and or warming the waters to force the density to fit the simple end-member model.

Near Patton and Warwick seamounts, the salinity and density that defines NPIW occurs at the base of the halocline: ~150-200m at Patton and 185-350m at Warwick. The thick ~33.9 psu water mass and salinity inflection observed in the vertical profile at Warwick leaves no doubt as to the occurrence of NPIW, whereas at Patton the layer is rather thin. $\Delta^{14}C$ values of thermocline and NPIW waters at Warwick are higher than similar density (salinity) waters to the north as observed at Patton. This observation could be interpreted as more bomb-^{14}C in the ventilated waters around Warwick Seamount compared to sub-halocline central gyre waters to the north. An equally valid statement would be that the central Alaskan Gyre waters has diluted its "bomb-^{14}C" signature to a greater extent with low ^{14}C water. At depths deeper than NPIW the waters sampled by the two hydrocasts are indistinguishable in density (salinity) $\Delta^{14}C$ space. Subtropical surface waters are the likely source of the higher ^{14}C signature observed at Warwick relative to Patton. Subtropical (higher-^{14}C) waters would be entrained into the southern edges of the Alaskan gyre through interaction with the North Pacific Current.

Relative to the (spatially) equivalent WOCE P16 (58) and P17 (127) stations, waters in the Gulf of Alaska (Patton) in 2002 have lower $\Delta^{14}C$ for a given potential density (σt) than those in the early 1990s (Figure 7). Indeed, none of the WOCE $\Delta^{14}C$ profiles approach the consistently low values observed at Patton for densities less than ~26.7σt and for the most part the same can be said for the transition or gyre boundary at Warwick. Comparison of our $\Delta^{14}C$ data to GEOSECS indicates erosion of the transient bomb-^{14}C signature to a density of ~26.8 or a depth of ~160 meters at station 218 (50.43N 176.58W). In June of 1982 Gulf of Alaska surface water $\Delta^{14}C$ values approached 100‰ at a latitude of 51.5°N (Stuiver and Quay, 1982). By the late 1980s surface water $\Delta^{14}C$ had decreased to a maximum of ~70‰ with the highest values again around 50°N (Takahashi *et al.*, 1991). Values observed in the early 1990s as part of WOCE continue the trend towards lower $\Delta^{14}C$. The surface data document a steady erosion of the bomb-^{14}C transient from the 1970s to present.

In the north Pacific, pre-bomb $\Delta^{14}C$ surface water values are thought to be lower in the western sub-polar North Pacific where low-^{14}C water is entrained into the surface

mixed layer through vigorous vertical mixing and upwelling (c.f. Guilderson *et al.*, 2000). $\Delta^{14}C$ values in the eastern sub-polar North Pacific are more positive, likely due in part to entrainment of higher ^{14}C subtropical water from the North Pacific Current. Transport of western North Pacific waters would be accommodated in the North Pacific Current. Pre-bomb surface values over Warwick Seamount are inferred to be ~-105‰ (Roark et al., 2005), but as of yet we do not know what the values should be in the Alaskan Gyre itself. Our observation of decreasing $\Delta^{14}C$ surface values through the gyre in addition to lower $\Delta^{14}C$ in sub-thermocline water (NPIW) in the north versus the south implies a local source of low ^{14}C water. Chlorofluorocarbon ages indicate a residence time in the Alaskan Gyre of only a few years (Aydin et al., 1998). This precludes our observation being the result of in situ ageing. The likely mechanism is entrainment of low-^{14}C water and vertical exchange. Based on our data alone we cannot discount replenishment of surface and sub-thermocline waters with recently upwelled low-^{14}C water from the NW Pacific. It is possible that both physical mechanisms have contributed to the erosion of the bomb-^{14}C transient in the Gulf of Alaska.

The observation that the lowest $\Delta^{14}C$ and hence radiocarbon age is not coincident with lowest oxygen concentrations indicates a decoupling between oxygen concentration (or apparent oxygen utilization) and ventilation age. This would be caused by high oxygen consumption during remineralization of organic matter along the margin of northern North America and within the water column under areas of high productivity.

"Ultra-Precision" 14C Analyses

The average fractional error of the thirty-three pairs of carefully "split" CO_2 and individually graphitized targets is 0.94‰. To the best of our knowledge, these are the first ~1‰ AMS results on real-world samples. These results indicate that with high negative ion sputter efficiency and complete beam transport that it is possible to achieve results comparable to the best liquid scintillation laboratories. In this experiment we did not see the deleterious and potentially limiting effects described by Nadeau et al., (1987; 1990). We believe that this observation is the result of individual AMS-system and ion

source peculiarities. The CAMS spectrometer system was designed with performance and capabilities not available in commercially available AMS systems or similar systems at many nuclear physics laboratories. All high energy magnets have 5cm apertures and all quadrapole lenses in the beam-line have 10cm apertures. This results in better optics with complete transmission and no fractionation [Davis *et al.*, 1990; Davis *et al.*, 1992]. Unlike many other cesium sputter sources, the CAMS system does not seem to introduce appreciable time-dependent fractionation during the course of analyzing indvidual targets or at variable ion currents [Southon *et al.*, 1991]. Due to the design of the low energy injection system, no beam is lost even at high source emittance. All this being said, the true test of this type of measurements is not as a "one-off" but long-term reproducibility with precision and accuracy.

CONCLUSIONS

Radiocarbon measurements on total dissolved inorganic carbon on water samples from the Gulf of Alaska obtained in 2002 have been compared with similar data from the 1990s (WOCE), the 1970s (GEOSECS), and surface water samples of opportunity taken in the 1980s. The open gyre surface water values are 20-40‰ more negative than those documented in 1991 and 1993 (WOCE) continuing the trend towards lower $\Delta^{14}C$ values since GEOSECS. Within the admittedly limited spatial sampling, erosion of the bomb-^{14}C transient appears from the surface to densities approaching 26.8σt. In addition to lateral (isopycnal) replenishment with waters from the western Pacific via the general shallow circulation, our data imply a local source of low-^{14}C water. Vertical mixing and entrainment of water below 26.8σt is the preferred source of the low-^{14}C water. This interpretation would be consistent with other tracer data (e.g., Aydin et al. 1998).

In a proof of principle study, we took advantage of a sub-set of the samples to analyze to a level approaching 1‰. Individually graphitized splits of the same CO2 ampoules were analyzed on the same and different wheels. The vast majority replicated to 1‰ at 1-sigma over a range of values from ~-240 to ~0 ‰. The cumulative fractional error of the 33 "pairs" was 0.94‰. The results of this experiment indicate that AMS has

the potential to equal the precision and accuracy of high-precision liquid scintillation counting laboratories.

Acknowledgements: *This research was funded by the NOAA Office of Ocean Exploration (NA16RP2637). Sample preparation and assistance at UW by J Stutsman. We thank the captain and crew of the R/V Atlantis, and all members of the GoASEx science party. This manuscript benefited from discussions with T Brown and T Shirley. Radiocarbon analyses were performed under the auspices of the U.S. Department of Energy by the University of California Lawrence Livermore National Laboratory (contract W-7405-Eng-48).*

REFERENCES

Aydin M., Top Z, Fina RA, Olson DB, 1998. Modification of the intermediate waters I the northeastern subpolar Pacific. *J. Geophys. Res.*, 103, 30923-30940.

Bevington PR, Robinson DK, 1992. *Data reduction and error analysis for the physical sciences* 2nd edition, McGraw-Hill, Boston MA, USA 328pp

Davis JC, *et al.*, 1990. LLNL/UC AMS facility and research program. *Nuclear Instrument and Methods in Physics Research, Sect. B*, 52, 269-272.

Davis, J.C., *et al.*, 1992. Ion beam and isotopic analysis tools at Livermore. 3rd International Conference on Applications of Nuclear Techniques, Mykonos, Greece.

Donahue DJ, Linick TW, Jull AJT, 1990, Isotope-ratio and background corrections for accelerator mass spectrometry radiocarbon measurements. *Radiocarbon* 32, 135-142

Guilderson TP, Caldeira K, Duffy PB., 2000. Radiocarbon as a diagnostic tracer in ocean and carbon cycle modeling. *Global Biogeochemical Cycles,* 14, 887-902.

Key, R. M., et al., WOCE AMS radiocarbon I: Pacific Ocean results (P6, P16, and P17), Radiocarbon, 38, 425-518, 1996.

Monterey GI, Levitus S., 1997. *Seasonal Variability of Mixed Layer Depth for the World Ocean*. NOAA NESDIS Atlas 14, U.S. Gov. Printing Office, Wash., D.C.

Nadeau MJ, Litherland AE. 1990. Electric dissociation of negative ions. *Nuclear Instruments and Methods in Physics Research B* 52:387–90.

Nadeau MJ, Kieser WE, Buekens RP, Litherland AE. 1987. Quantum mechanical effects on sputter source isotope fractionation. *Nuclear Instruments and Methods in Physics Research B* 29:83–6.

Reid, J, Arthur RS., 1975. Interpretation of maps of geopotential anomaly for deep Pacific Ocean. *Journal of Marine Research*, 33, 37-52 Suppl.

Roark EB, *et al*., 2004. Radiocarbon based ages and growth rates of bamboo corals from the Gulf of Alaska. *Geophysical Research Letters* in review.

Southon JR, The calculation of 14C ages from AMS 14C/13C ratio measurements. Unpublished document

Southon. JR., *et al*., 1991. Progress in AMS measurements at the LLNL spectrometer. 14th International Radiocarbon Conference Proceedings, Tucson AZ.

Stuiver M, Polach H., 1977. Discussion of reporting of 14C data. *Radiocarbon* 19, 355-363.

Stuiver M, Quay PD., 1982 data published in: Reeburgh WS, Kipphut, GW 1986. Chemical distributions and signals in the Gulf of Alaska, its coastal margins and estuaries. NOAA/USDI Alaska OCS study # MMS 86-0095, Minerals Management Service, US Dept of the Interior.

Sverdrup HU, Johnson MW, Fleming RH., 1942. *The Oceans*. Prentice-Hall Englewood Cliffs, NJ, 1087pp

Takahashi T, Goddard J, Sutherland SC, Mathieu G, and Chipman DW., 1991. Assessment of carbon dioxide sink/source in the North Pacific Ocean: seasonal and geographic variability, 1984-1989. Final report for DOE contract 19X-SC428C, submitted to CDIAC, Environmental Sciences Div., Oak Ridge National Lab, Oak Ridge, TN 37939

Takahashi T, *et al*., 1997. Global air-sea flux of CO2: An estimate based on measurements of sea-air pCO_2 difference, *Proceedings National Academy of Sciences*, *94*, 8292-8299, 1997.

Talley LD, 1993. Distribution and formation of North Pacific Intermediate Water. *J. Physical Oceanography* 23, 517-537.

Talley LD, 1991. An Okhotsk Sea water anomaly: implications for ventilation in the North Pacific. *Deep Sea Research* Supp 38:S171-S190

Talley LD, Joyce TM, deSzoeke RA., 1991. Transpacific sections at 47°N and 152°W: distribution of properties. *Deep Sea Research* Supp 38:S63-S82

Tsunogai S, Watanabe S, Honda M, Aramaki T., 1995. North Pacific Intermediate Water studied chiefly with radiocarbon. *Journal of Oceanography* 51:519-536.

Van Scoy KA, et al., 1991a. Two decades of mixing tritium into the North Pacific Ocean. *Deep Sea Research Part A*, 38, suppl, S191-S219.

Van Scoy KA, et al., 1991b. Ventilation of North Pacific Intermediate Waters,: The role of the Alaskan Gyre, *Journal of Geophysical Research*, 96, 16801-16810.

Vogel JS, Southon JR, Nelson DE, 1987. Catalyst and binder effects in the use of filamentous graphite for AMS. *Nuclear Instruments and Methods in Physics Research, Sect.B*, 29, 50-56.

Warner MJ, Bullister JL, Wisegarver DP, Gammon RH, Weiss RF, 1996. Basin-wide distribution of chloroflurocarbons CFC-11 and CFC-12 in the North Pacific: 1985-1989. *Journal of Geophysical Research* 101:20,525-20,542

Watanabe YW, Harada K, Ishikawa K., 1994. Chlorofluorocarbons in the central North Pacific and southward spreading time of North Pacific Intermediate water. *Journal of Geophysical Research*, 99:25,195-25,213

Figure Captions

Figure 1 a) Winter sea level pressure (mbar) and surface currents, hatchured area is Aleutian Low. Cruise tracks of the R/V Thomas Thompson along nominal 47°N and 152°W are shown. b) Oxygen profile along 47°N. Contours are lines of potential density (σ_t) in kg/m^3. Note that the isopycnals slope down to the east. c) Salinity profile along 152°W, with lines of potential density overlain.

Figure 2 GoASEx underway sample (solid circles) locations relative to WOCE P16 (open triangles) and P17 (open circles) ^{14}C-stations. Fine contours are bathymetry. Solid black contours are climatological summer surface salinity (Levitus 1998). Thick dotted line is the zero-contour of the curl of the wind-stress based on May/June 2002 winds. GEOSECS station 218 is to the west of this region.

Figure 3 Sea surface temperature (SST, °C) and surface salinity (SSS, psu) as a function of latitude as observed in June/July of 2002.

Figure 4 a. Surface Δ^{14}C as a function of latitude during the summer of 2002 (solid circles), March of 1991 (P16, open triangles), and June of 1993 (P17, open circles). b. GoASEx surface Δ^{14}C as a function of density and latitude (water mass).

Figure 5 Patton (ATL 7-15 ctd1) and Warwick (ATL7-16 ctd2) hydrographic profiles to ~2200 meters: temperature (solid line), salinity (thin solid line), oxygen concentration (thick line) and Δ^{14}C (connected solid squares). Note the well-mixed Δ^{14}C surface layer trapped above the halocline and that the lowest Δ^{14}C values do not occur in the oxygen minimum zone.

Figure 6 Δ^{14}C results on CO_2 extracted from Gulf of Alaska sea water samples. Single ampoules of CO_2 were split to produce two independent graphitization targets and pairs were analyzed on the same and/or different sample wheels. The relative or fractional error of the 33 individual pairs scatter with a mean error of 0.94‰. The majority of pairs are analytically indistinguishable from each other at 1-sigma (sd).

Figure 7 Temporal evolution of Δ^{14}C in the Gulf of Alaska as a function of potential density. Snapshots include: 1991 (P16, open triangles), 1993 (P17, open circles), and 2002 (GoASEx, solid circles and for surface samples crosses). P17-127 (asterick) and P16-58 (star) are the two WOCE stations closest to that of Patton ATL07/15-ctd1. For reference we also plot GEOSECS station 218 (solid diamond: 176.58°W, 50.43°N) taken in the fall of 1973. Surface pre-bomb value at Warwick as reconstructed from biologic archives (Roark et al., 2005) is demarked by the solid arrow.

Figure 1

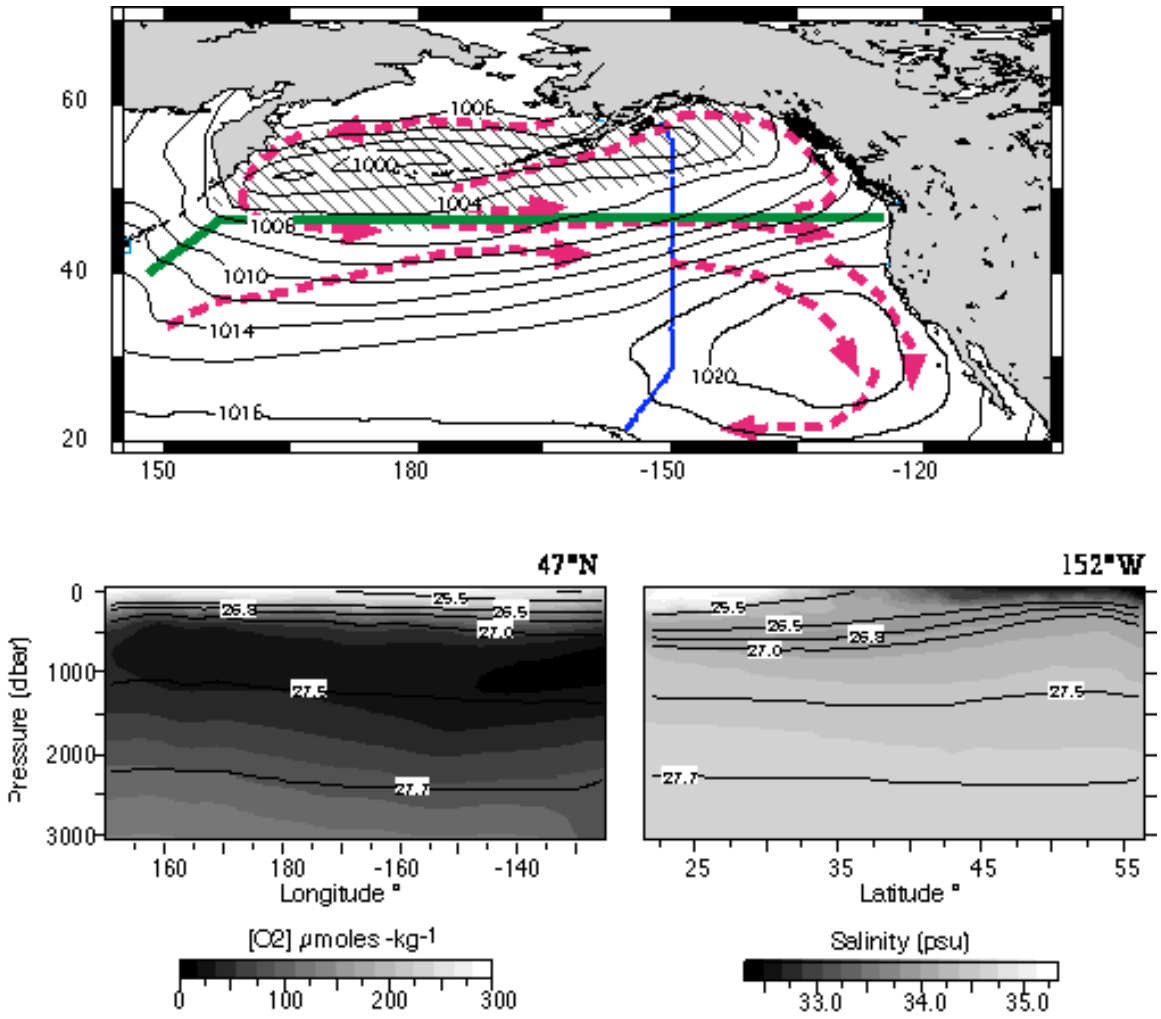
60
40
20
150
180
-150
-120
1006
1002
1004
1008
1010
1014
1020
1016
47°N
152°W
Pressure (dbar)
0
1000
2000
3000
25.5
26.5
27.0
27.5
27.7
160
180
-160
-140
Longitude °
25
35
45
55
Latitude °
[O2] μmoles-kg-1
0
100
200
300
Salinity (psu)
33.0
34.0
35.0

Figure 2

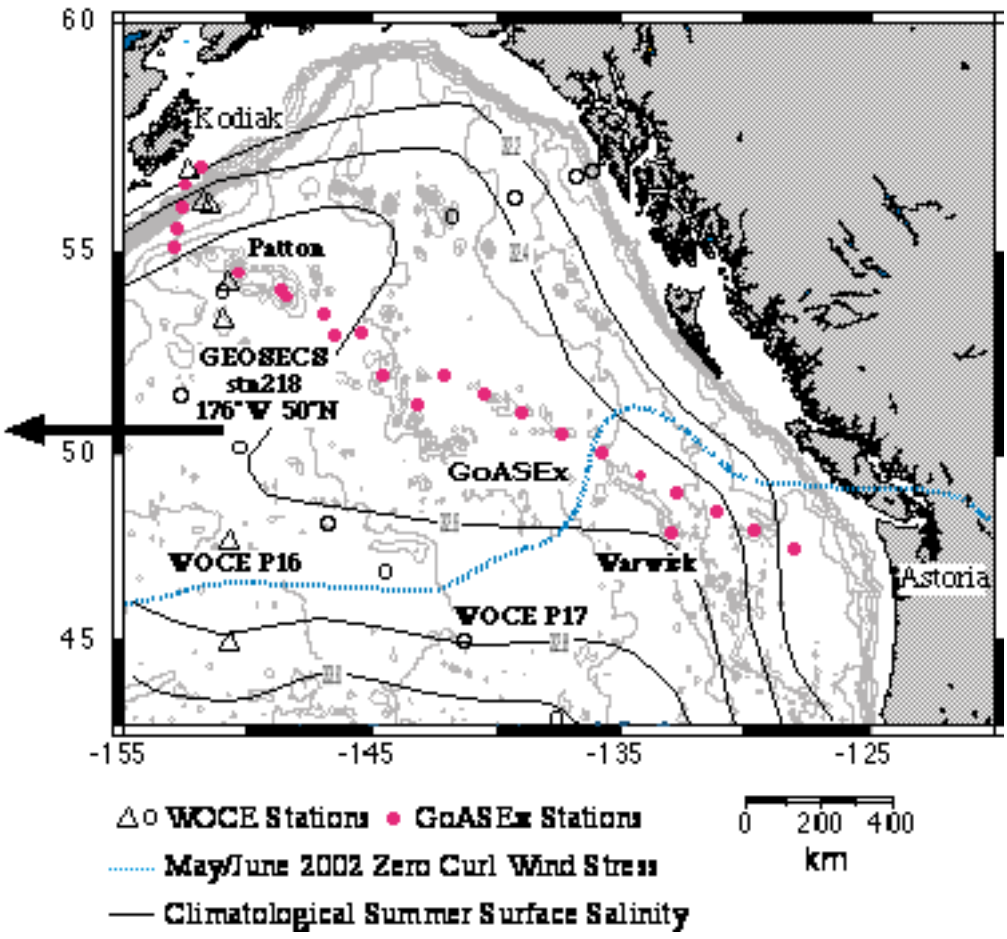
60
55
50
45
-155
-145
-135
-125
Kodiak
Patton
GEOSECS
sta218
176°W 50°N
GoASEx
WOCE P16
WOCE P17
Varwik
Astoria
△○ WOCE Stations ● GoASEx Stations
May/June 2002 Zero Curl Wind Stress
Climatological Summer Surface Salinity
0 200 400
km

Figure 3

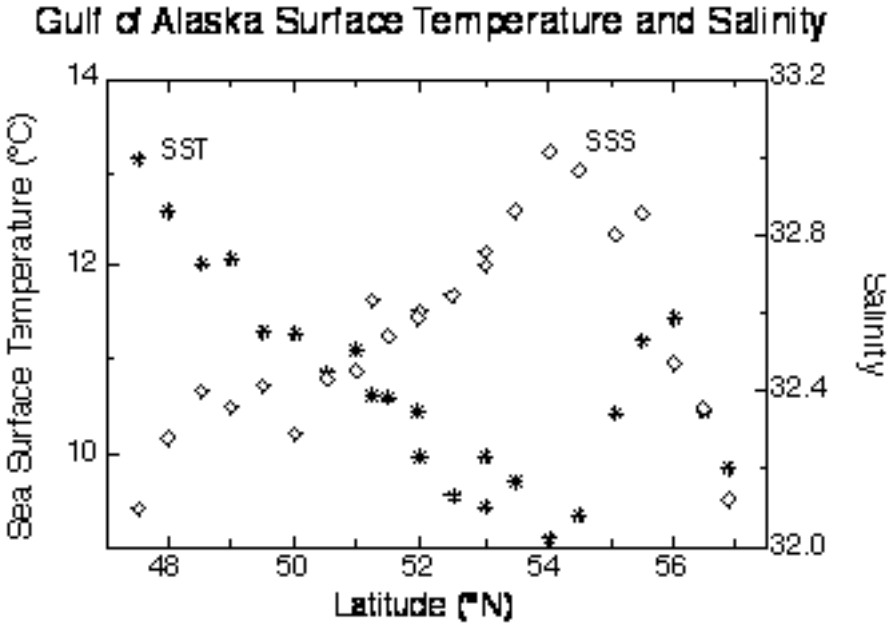
Gulf of Alaska Surface Temperature and Salinity
Sea Surface Temperature (°C)
Salinity
Latitude (°N)
SST
SSS
14
12
10
33.2
32.8
32.4
32.0
48
50
52
54
56

Figure 4

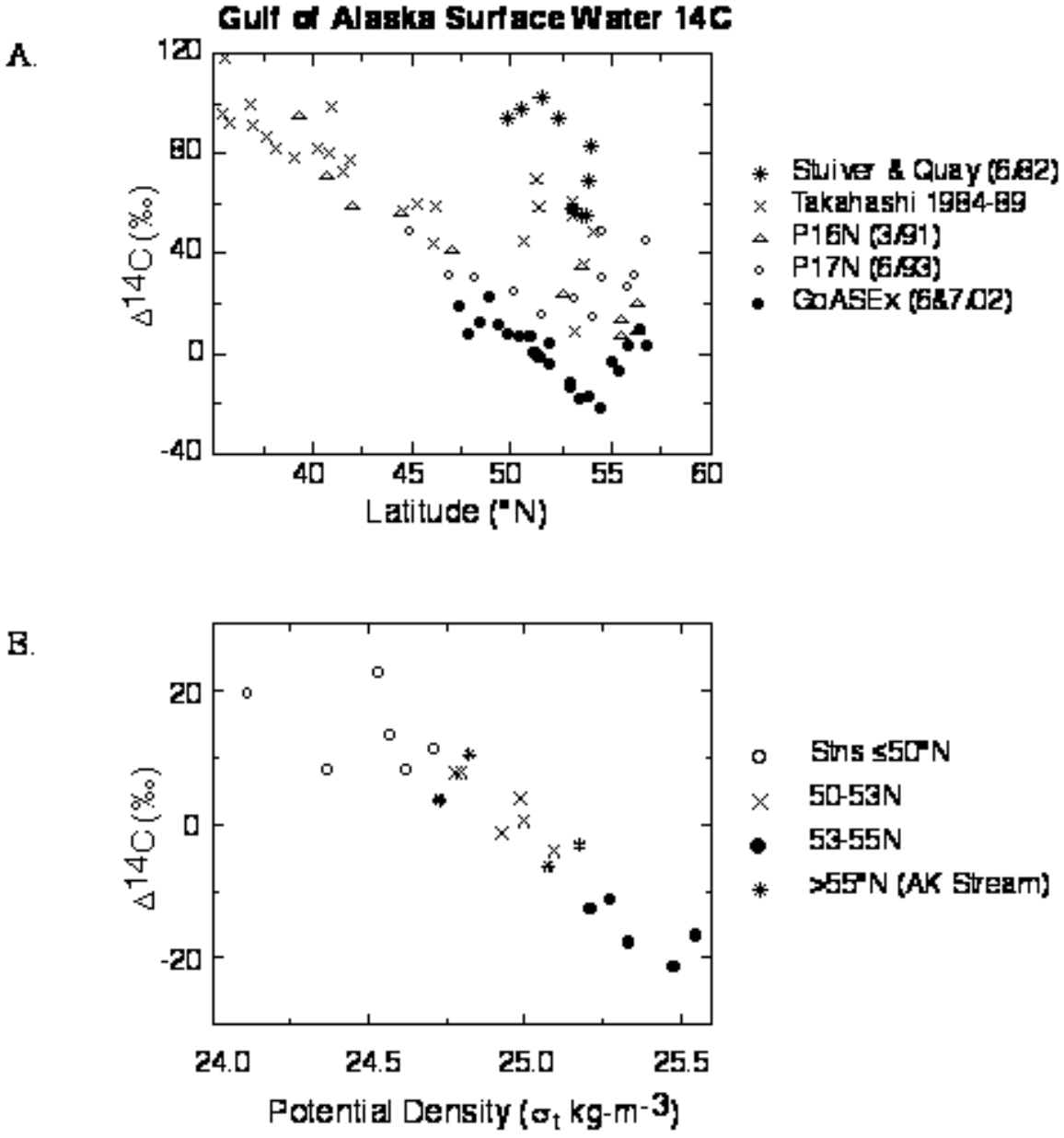
A.
Gulf of Alaska Surface Water 14C
Δ14C (‰)
Latitude (°N)
Stuiver & Quay (6/82)
Takahashi 1984-89
P16N (3/91)
P17N (6/93)
GoASEx (6&7/02)
B.
Δ14C (‰)
Potential Density (σt kg-m-3)
Stns ≤50°N
50-53N
53-55N
>55°N (AK Stream)

Figure 5

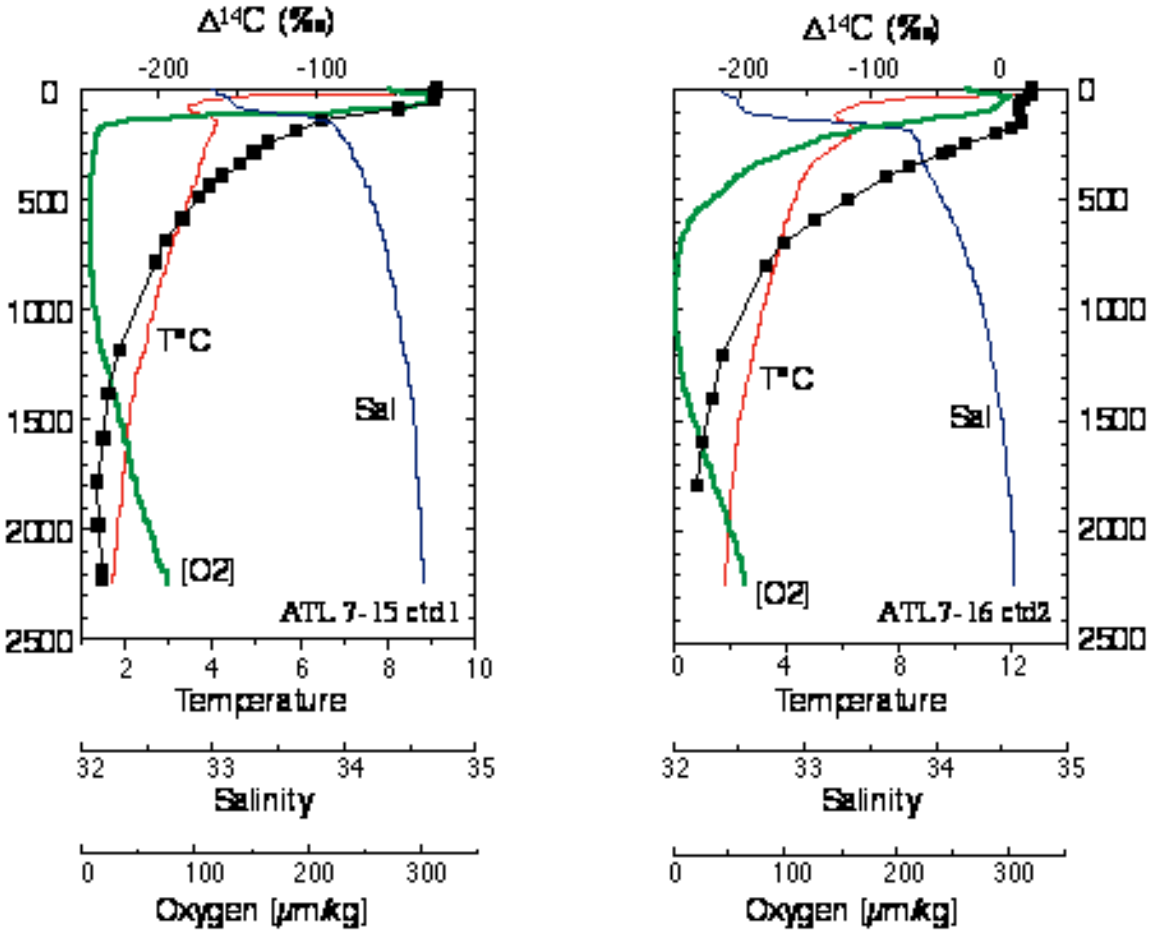
Δ14C (‰)
-200
-100
0
500
1000
1500
2000
2500
T°C
Sal
[O2]
ATL 7-15 ctd1
ATL 7-16 ctd2
2
4
6
8
10
12
Temperature
32
33
34
35
Salinity
0
100
200
300
Oxygen [µm/kg]

Figure 6

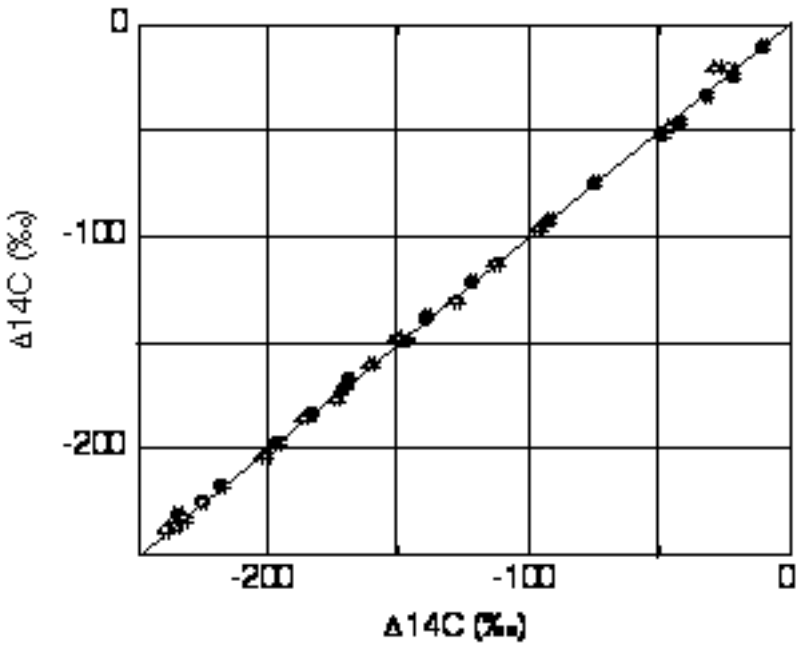

Figure 7

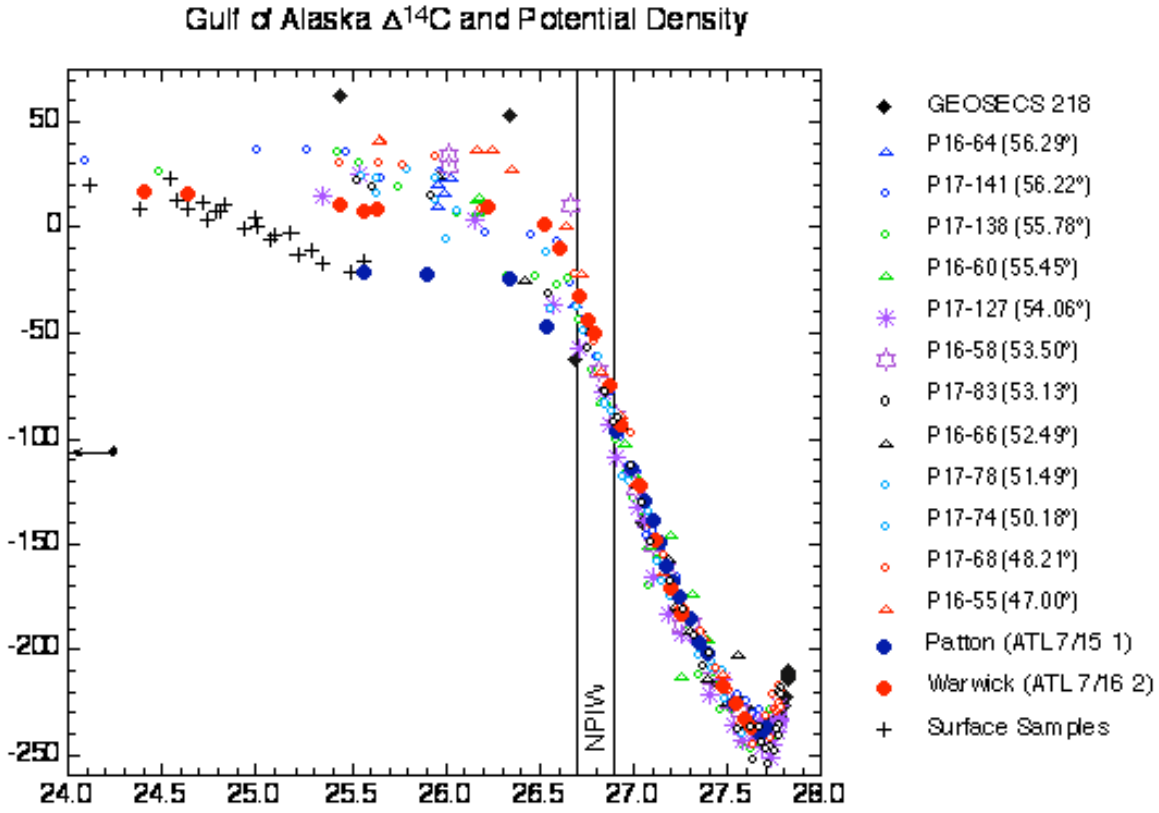
Gulf of Alaska Δ14C and Potential Density
50
0
-50
-100
-150
-200
-250
24.0
24.5
25.0
25.5
26.0
26.5
27.0
27.5
28.0
NPIW
GEOSECS 218
P16-64 (56.29°)
P17-141 (56.22°)
P17-138 (55.78°)
P16-60 (55.45°)
P17-127 (54.06°)
P16-58 (53.50°)
P17-83 (53.13°)
P16-66 (52.49°)
P17-78 (51.49°)
P17-74 (50.18°)
P17-68 (48.21°)
P16-55 (47.00°)
Patton (ATL7/15 1)
Warwick (ATL 7/16 2)
Surface Samples

Table 1. Surface water data.
Radiocarbon data are presented as absolute Fraction modern and (age-corrected) Δ14C.

Station ID	LAT	LON	SST (°C)	Salinity (psu)	Pot Den (kg-m-3)	δ13C	CAMS#	Abs Fmod	±Fm	Δ14C	±‰
ATL-7-15-2	47.50	128.04	13.16	32.10	24.11	2.12	93817	1.0262	0.0029	19.6	2.9
ATL-7-15-3	48.00	129.56	12.58	32.28	24.37	1.45	93818	1.0148	0.0040	8.3	4.0
ATL-7-15-4	48.51	131.09	12.03	32.40	24.57	1.57	93819	1.0196	0.0032	13.1	3.2
ATL-7-15-5	49.01	132.62	12.09	32.36	24.53	1.85	93820	1.0292	0.0029	22.6	2.9
ATL-7-15-6	49.50	134.14	11.31	32.41	24.71	1.41	93821	1.0179	0.0029	11.4	2.9
ATL-7-15-7	50.02	135.74	11.28	32.29	24.62	1.47	93822	1.0148	0.0041	8.3	4.1
ATL-7-15-8	50.50	137.27	10.86	32.43	24.80	1.50	93823	1.0140	0.0029	7.5	2.9
ATL-7-15-9	51.00	138.96	11.10	32.46	24.78	1.57	93824	1.0140	0.0029	7.5	2.9
ATL-7-15-10	51.50	140.47	10.59	32.54	24.93	1.47	93825	1.0053	0.0029	-1.1	2.9
ATL-7-15-11	52.00	142.11	9.96	32.60	25.09	1.32	93826	1.0024	0.0031	-4.0	3.1
ATL-7-15-12	52.50	143.75	9.55	32.65	25.19	1.28	Ampule lost@CAMS				
ATL-7-15-13	53.00	145.41	9.43	32.72	25.27	1.13	93827	0.9952	0.0028	-11.1	2.8
ATL-7-15-14	53.50	146.98	9.69	32.86	25.33	1.02	93828	0.9886	0.0028	-17.7	2.8
ATL-7-15-15	54.01	148.60	9.10	33.01	25.55	1.26	93829	0.9898	0.0028	-16.5	2.8
ATL-7-15-16	54.50	150.32	9.33	32.97	25.48	1.29	93830	0.9849	0.0031	-21.4	3.1
ATL-7-15-17	55.07	152.85	10.42	32.80	25.17	1.37	93831	1.0034	0.0028	-3.0	2.8
ATL-7-15-18	55.52	152.71	11.20	32.86	25.07	1.38	93832	1.0001	0.0028	-6.3	2.8
ATL-7-15-19	56.00	152.55	11.46	32.47	24.73	1.79	93833	1.0103	0.0043	3.8	4.3
ATL-7-15-20	56.50	152.38	10.44	32.36	24.82	1.71	93834	1.0168	0.0029	10.3	2.9
ATL-7-16-1	56.90	151.86	9.84	32.12	24.73	1.85	93835	1.0100	0.0028	3.5	2.8
ATL-7-16-2	53.01	146.52	9.97	32.76	25.21	1.14	93836	0.9936	0.0035	-12.8	3.5
ATL-7-16-3	51.98	144.50	10.44	32.59	24.99	1.38	93837	1.0104	0.0028	4.0	2.8
ATL-7-16-4	51.24	143.11	10.61	32.63	25.00	1.40	93838	1.0069	0.0029	0.5	2.9

Table 2.
Atlantis 7-15 CTD1 53° 56.00'N 148° 26.00'W (6/27/2002)
"Patton Seamount"

BTL	Depth (meter)	in situ T (°C)	Salinity (psu)	Pot Den (kg/m-3)	Oxygen (μm/kg)	δ13C (‰)	CAMS #	Abs FM	±Fm	Δ14C	±	CAMS#	Abs Fm	±Fm	Δ14C	±
24	0	9.20	33.00	25.57	276.4	1.15	93839†	0.9769	0.0015	-23.1	1.5	93840†	0.9855	0.9792	-20.8	1.5
23	25	7.13	33.05	25.91	301.1	1.02	94151†	0.9784	0.0012	-21.6	1.2	94152†	0.9819	0.9757	-24.3	1.0
22	50	3.90	33.13	26.35	310.8	0.53	94154†	0.9721	0.0011	-27.9	1.1	94375¥	0.9861	0.9798	-20.2	1.4
21	100	3.51	33.34	26.55	229.8	0.00	94153†	0.9544	0.0011	-45.6	1.1	94374¥	0.9578	0.9517	-48.3	1.2
20	150	4.06	33.88	26.92	31.5	-0.82	94155†	0.9043	0.0011	-95.7	1.1	94376¥	0.9094	0.9036	-96.4	1.2
19	200	4.00	33.97	27.00	14.8	-0.85	94156†	0.8872	0.0011	-112.8	1.1	94377¥	0.8921	0.8864	-113.6	1.2
18	250	3.85	34.03	27.07	13.5	-0.82	94157†	0.8716	0.0009	-128.4	0.9	94378¥	0.8744	0.8689	-131.1	1.2
17	300	3.77	34.07	27.11	12.6	-0.79	94158†	0.8603	0.0011	-139.7	1.1	94159†	0.8671	0.8617	-138.3	1.0
16	350	3.70	34.11	27.15	11.2	-0.77	94160†	0.8502	0.0009	-149.8	0.9	94379¥	0.8583	0.8529	-147.1	1.2
15	400	3.64	34.15	27.18	10.2	-0.76	94161†	0.8403	0.0010	-159.7	1.0	94380¥	0.8453	0.8400	-160.0	1.0
14	450	3.53	34.19	27.22	9.7	-0.46	94162†	0.8314	0.0009	-168.6	0.9	94163†	0.8382	0.8329	-167.1	0.9
13	500	3.46	34.21	27.25	9.0	-0.74	94164†	0.8266	0.0009	-173.4	0.9	94381¥	0.8290	0.8237	-176.3	1.1
12	600	3.28	34.26	27.31	8.0	-0.74	94165†	0.8147	0.0009	-185.3	0.9	94382¥	0.8197	0.8145	-185.5	1.1
11	700	3.09	34.31	27.36	8.3	-0.74	94166†	0.8041	0.0009	-195.9	0.9	94167†	0.8079	0.8028	-197.2	0.9
10	800	2.94	34.34	27.40	10.0	-0.78	94168†	0.7989	0.0009	-201.1	0.9	94383¥	0.8017	0.7966	-203.4	1.0
9	1000	2.67	34.41	27.48	13.3	-0.89	no CO2									
8	1200	2.43	34.46	27.54	20.3	-0.67	94384†	0.7750	0.0010	-225.0	1.0	94385†	0.7793	0.7743	-225.7	1.0
7	1400	2.17	34.52	27.60	30.9	-0.59	94386†	0.7658	0.0010	-234.2	1.0	94387†	0.7732	0.7683	-231.7	1.0
6	1600	2.03	34.55	27.64	40.7	-0.62	94388†	0.7646	0.0010	-235.4	1.0	94389†	0.7676	0.7628	-237.2	1.0
5	1800	1.93	34.57	27.67	49.6	-0.54	94390†	0.7604	0.0010	-239.6	1.0	94391†	0.7656	0.7608	-239.2	1.0
4	2000	1.81	34.59	27.69	63.0	-0.51	94392¥	0.7614	0.0010	-238.6	1.0	94551•	0.7662	0.7613	-238.7	2.3
3	2200	1.71	34.61	27.72	77.3	-0.37	94552•	0.7627	0.0023	-237.3	2.3	94553•	0.7681	0.7633	-236.7	2.3
2	2250	1.70	34.61	27.72	78.1	-0.11	94554•	0.7631	0.0023	-236.9	2.3	94555•	0.7673	0.7624	-237.6	2.0

One meter average upcast temperature, salinity, oxygen averaged over 3m interval centered on bottle firing.

† = ~1E6 14C events
¥ = ~7.5E5 14C events
• = normal precision

Table 3.
Atlantic 7-16 CTD2 47° 57.00N 132° 55.00'W (7/10/2002)
"Warwick Seamount"

BTL	Depth (meter)	in situ T (°C)	Salinity (psu)	Pot Den (kg/m-3)	Oxygen (μm/kg)	δ13C (‰)	CAMS #	Abs FM	±Fm	Δ14C	±	CAMS#	Abs Fm	±Fm	Δ14C	±
24	3	12.95	32.38	24.42	263.5	1.74	94556•	1.0167	0.0043	16.7	4.3	94557•	1.0180	0.0030	18.0	3.0
23	25	11.78	32.40	24.65	273.6	1.65	94558•	1.0182	0.0030	18.2	3.0	94559•	1.0147	0.0025	14.7	2.5
22	50	7.28	32.49	25.45	300.3	1.41	94560•	1.0089	0.0025	8.9	2.5	94561•	1.0124	0.0030	12.4	3.0
21	75	6.44	32.50	25.57	292.1	1.22	94562•	1.0103	0.0030	10.3	3.0	94563•	1.0051	0.0025	5.1	2.5
20	100	5.98	32.54	25.65	287.6	1.05	94564•	1.0141	0.0030	14.1	3.0	94565•	1.0039	0.0027	3.9	2.7
19	150	6.13	33.30	26.24	223.4	0.42	94566•	1.0081	0.0030	8.1	3.0	94567•	1.0109	0.0033	10.9	3.3
18	175	6.41	33.73	26.54	180.1	0.11	94568•	1.0000	0.0030	0.0	3.0	94569•	1.0020	0.0032	2.0	3.2
17	200	6.37	33.82	26.62	161.0	-0.03	94118†	0.9898	0.0015	-10.2	1.5	94119†	0.9898	0.0012	-10.2	1.2
16	250	5.84	33.87	26.72	126.3	-0.23	94120†	0.9685	0.0011	-31.5	1.1	94121†	0.9666	0.0012	-33.4	1.2
15	275	5.52	33.88	26.77	111.2	-0.30	94122†	0.9580	0.0010	-42.0	1.0	94123†	0.9535	0.0011	-46.5	1.1
14	300	5.32	33.89	26.80	98.5	-0.35	94124†	0.9515	0.0013	-48.5	1.3	94125†	0.9479	0.0010	-52.1	1.0
13	350	4.81	33.92	26.88	73.9	-0.49	94126†	0.9249	0.0010	-75.1	1.0	94127†	0.9250	0.0010	-75.0	1.0
12	400	4.58	33.97	26.94	59.3	-0.42	94128†	0.9075	0.0010	-92.5	1.0	94129†	0.9073	0.0010	-92.7	1.0
11	500	4.28	34.05	27.04	38.0	-0.62	94130†	0.8780	0.0012	-122.0	1.2	94131†	0.8783	0.0009	-121.7	0.9
10	600	4.00	34.13	27.13	16.7	-0.70	94132†	0.8524	0.0010	-147.6	1.0	94133†	0.8517	0.0009	-148.3	0.9
9	700	3.79	34.20	27.21	8.5	-0.71	94134†	0.8300	0.0009	-170.0	0.9	94135†	0.8291	0.0010	-170.9	1.0
8	800	3.60	34.26	27.27	4.7	-0.71	94136†	0.8168	0.0009	-183.2	0.9	94137†	0.8165	0.0010	-183.5	1.0
7	1000	3.16	34.36	27.39	3.9	-0.69	no CO2									
6	1200	2.81	34.43	27.48	7.5	-0.70	94138†	0.7824	0.0009	-217.6	0.9	94139†	0.7824	0.0010	-217.6	1.0
5	1400	2.48	34.48	27.55	13.6	-0.67	94140†	0.7751	0.0008	-224.9	0.8	94141†	0.7747	0.0008	-225.3	0.8
4	1600	2.24	34.52	27.60	25.8	-0.63	94142†	0.7655	0.0008	-234.5	0.8	94143†	0.7692	0.0013	-230.8	1.3
3	1800	2.07	34.56	27.64	37.9	-0.54	94144†	0.7628	0.0008	-237.2	0.8	94145†	0.7630	0.0008	-237.0	0.8
2	2200	1.82	34.60	27.70	64.7	-0.38	no CO2									

One meter average upcast temperature, salinity, oxygen averaged over 3m interval centered on bottle firing.

† = ~1E6 14C events
¥ = ~7.5E5 14C events
• = normal precision